5*S*-5*D* two-photon transition in rubidium vapor at high densities

K. Hassanin,[1] P. Federsel,[2] F. Karlewski,[2] and C. Zimmermann[1,*]
[1]*Physikalisches Institut, Eberhard-Karls-Universität Tübingen, Auf der Morgenstelle 14, D-72076 Tübingen, Germany*
[2]*HighFinesse GmbH, Wöhrdstraße 4, D-72072 Tübingen, Germany*

(Received 10 October 2022; revised 3 February 2023; accepted 20 March 2023; published 5 April 2023)

The rubidium 5*S*-5*D* Doppler-free two-photon transition has been observed in a thermal vapor cell by detecting the infrared radiation emitted during the decay from the 5*D* excited level to the 5*P* intermediate level. Different to the usual detection scheme based on blue light emission this approach does not suffer from reabsorption and still works at high densities. This not only allows for a dramatically enhanced detectable emission rate but also for investigating collisional effects such as collisional broadening and collisional energy transfer. Furthermore, we observe a yet unknown temperature dependence of the resonance linewidth for transitions into the states of the $5D_{5/2}$ level. Consequences for the design of an optical Rb-frequency standard are discussed.

DOI: 10.1103/PhysRevA.107.043104

I. INTRODUCTION

The optical two-photon transition from the rubidium 5*S*-ground level to the excited 5*D* level has been extensively studied in the past, mainly because of its potential use as a secondary optical frequency standard [1–3]. Such instruments are interesting in optical telecommunication [4] but also miniaturized and portable versions for applications in space are discussed [5–7]. The long lifetime of the 5*D* states [8] and Doppler-free excitation with counterpropagating laser beams allows for an observed linewidth of less than 1 MHz [1] and fractional frequency stability on the order of 10^{-13} has been reported recently [5]. In these advanced experiments, the ac Stark shift [9] inhibits further improvement, curable either by even better stabilization of the laser power or by improved detection efficiency. A revision of the standard detection method for the two-photon transition might be helpful here.

The conventional detection scheme observes the 5*S*-5*D* transition by collecting blue light emitted during the decay cascade from the 5*D* excited level to the 5*S* ground level via the 6*P* level (see Fig. 1). In thermal vapor cells the observable blue emission increases linearly with atomic density until the gas gets optically thick and the emitted blue light is reabsorbed by the gas in the area between the laser defined excitation volume and the cell wall [4]. In this paper we explore an alternative scheme which overcomes this density limitation by detecting the infrared light emitted during the optical decay from 5*D* to the intermediate 5*P* level [8]. This light cannot be reabsorbed since the atoms between the excitation volume and the cell wall are in the 5*S* ground state. A reabsorbing transition from 5*P* to 5*D* is thus not possible and the gas remains optically transparent for the detected infrared light even at high densities. The detection efficiency can now be enhanced by increasing the cell temperature resulting in higher density and consequently higher emission. Furthermore, infrared detection also benefits from the branching ratio of the 5*D* decay channels. First, the decay rate to the 5*P* level is a factor of 1.5 stronger than the decay into the 6*P* level, and second, only one third of the 6*P* population directly decays into the ground state emitting blue light. In total, the emitted infrared photon rate is 4.6 times higher than the emitted blue photon rate. This together with the suppressed reabsorption allows us to observe an increase of the observable emission power by almost two orders of magnitude at high densities.

II. EXPERIMENTAL SETUP

The experimental setup is shown in Fig. 2. The atoms are excited by an external cavity diode laser (Toptica, DL pro) with a wavelength near 778 nm. We determined its emission spectrum with a commercial linewidth analyzer (HighFinesse, LWA 1k) and find a Gaussian line shape with an effective linewidth of 400 kHz at 778 nm. The laser output is spatially filtered by a polarization maintaining single mode fiber, the beam radius is adjusted with a telescope, and, after passing a polarizing beam splitter and a quarter wave plate, 25 mW of circularly polarized light is focused into a 75-mm-long rubidium cell containing a natural isotope mixture. The beam radius at the focus in the cell amounts to $w_0 = 75$ μm. This is a reasonable compromise between high intensity to maximize the two-photon transition rate and small time of flight broadening. Since we are mainly investigating the detection scheme here, we do not take into account light shifts and other systematic effects, which are certainly important for the design of an optimized frequency standard. After passing the cell, the light is recollimated with a lens and retroreflected by a plane mirror. The cell is heated in a two-chamber oven with a controlled cold spot to avoid rubidium condensation at the cell windows. The temperature of the cold spot is monitored with a thermistor (PT1000) and used to derive the atom density in the cell [11]. The rest of the cell is about 2% hotter than the cold spot. The temperature at different test points at the cell surface varies by less than 1%. We take data at temperatures

*Corresponding author: claus.zimmermann@uni-tuebingen.de

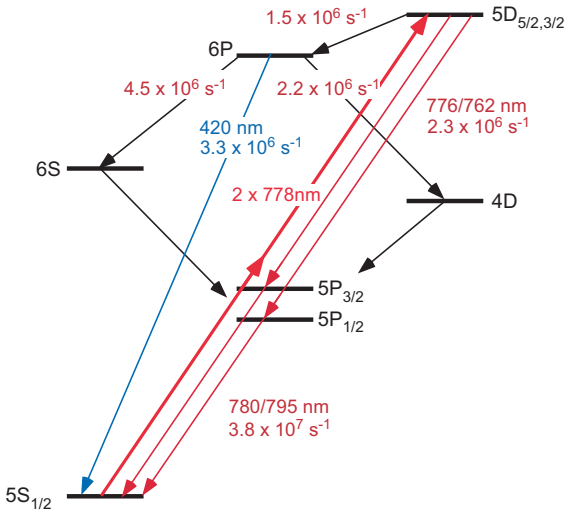

FIG. 1. Two-photon spectroscopy of the 5*D* states of rubidium. Simplified scheme of the relevant levels. The two fine-structure components of the 5*D* level are separated by an energy of *h*90 GHz and can both be excited with our laser setup (*h* is Planck's constant). The states of the 5*D* level decay either via 6*P* to the ground state emitting blue light or directly to the 5*P* level emitting infrared light. Wavelengths and decay rates are taken from [10].

between 347 and 500 K corresponding to densities between 1×10^{18} and 2.5×10^{21} m^{-3}.

The light emitted from the cell is collected and collimated by a first lens, filtered by an appropriate dielectric filter, and refocused into the detector. For detecting the blue emission from the 6*P* level near 420 nm we use a short pass filter (Thorlabs FESH0450, 98% transmission at 420 nm). It suppresses laser stray light and all infrared atomic emission. For detecting the infrared emission near 762 nm caused by the decay into the intermediate $5P_{1/2}$ level we use a 10-nm-wide bandpass filter (Asahi Spectra ASA XBPA760, 98% transmission at 760 nm). Detecting the decay into the intermediate $5P_{3/2}$ level is more tricky since the wavelength of the emitted light near 776 nm is close to the laser wavelength near 778 nm. We thus use two filters. A first 10-nm-wide bandpass filter at 780 nm (Thorlabs FL780-10, 71% transmission at 778 nm and 33% transmission at 776 nm) suppresses unwanted blue and

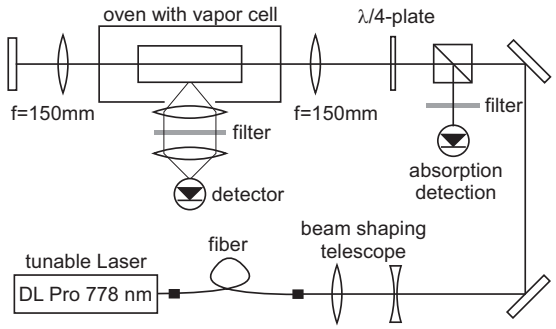

FIG. 2. Experimental setup. It differs from the standard setup only by the filter set in front of the photomultiplier. For details see text.

infrared atomic emission. A second filter (Laser Components LC-785USSP-25) separates the wanted atomic emission from laser stray light. It is designed as an ultrasteep short pass filter with a cutoff wavelength at 785 nm. We tune the edge of the filter spectrum by slightly tilting the filter such that as much scattered light is suppressed without losing atomic emission. The insertion loss of this second filter remains below 5%. By this way the average stray light offset can be suppressed to the level of the observed signal. This method is not perfect and we have to accept a larger background noise as compared to the detection schemes at 762 nm and in the blue. The atomic emission is detected with a silicon photomultiplier with integrated transimpedance amplifier (SiPM, PM3315-WB-B0 from KETEK). It is made of 38 800 single-photon avalanche photodiodes, integrated on a silicon substrate. The linear size of each microcell is 15 μm and the active area is 3×3 mm^2. Its photon detection efficiency amounts to 30% at 420 nm and 4% at 780 nm. The detector is not optimized for detecting infrared emission. For the construction of a two-photon transition frequency standard detectors with better efficiency are available. The detector output was recorded with a PicoScope 5442D USB oscilloscope with a digital low-pass filter at 800 kHz to suppress high-frequency noise generated by the SiPM. The product of the detector efficiency and the filter transmission amounts to 0.29, 0.039, and 0.013 for detecting emission at 420, 762, and 776 nm.

III. EMISSION

We observe transitions into the hyperfine multiplets of the $5D_{3/2}$ level and the $5D_{5/2}$ level by tuning the laser across the spectrum at a rate of 30 MHz/ms and detecting the atomic emission with a temporal resolution of 6 μs. Examples are shown in Fig. 3. The plotted power has been corrected for filter transmission and detector efficiency. It represents the power emitted by the atoms into the solid angle of detection. Each multiplet is analyzed by fitting a sum of four individual Lorentz functions to the recorded spectrum. The deviations from the more correct Voigt profiles have been checked to be negligible. Background due to stray light was also determined by the fit procedure and subtracted from the data. The maximum of the fit function for each resonance was plotted for various densities, which have been determined from the vapor pressure given by the temperature of the cold spot. Here, we discuss the transitions from the $5S_{1/2}$, $F = 2$ hyperfine ground state of ^{87}Rb into the two strongest components of each hyperfine multiplet, which are the transitions into $F = 4$ and 3 of the $5D_{5/2}$ level (in the following called "5/2 excitation") and into $F = 2$ and 3 of the $5D_{3/2}$ level ("3/2 excitation").

Figure 4 summarizes the main result. The two lower curves ("blue emission") are recorded with the conventional method of detecting the blue emission near 420 nm. For 3/2 excitation the emission is significantly weaker than for 5/2 excitation. This is because the 3/2 excitation is resonantly enhanced mainly by the states of the $5P_{1/2}$ intermediate level, which is detuned relative to the laser by 15 nm. The states relevant for the 5/2 excitation belong to the $5P_{3/2}$ intermediate level which is detuned by only 2 nm [1].

The three upper curves contain the main results observed in this paper. The 3/2 excitation is recorded with the filter for

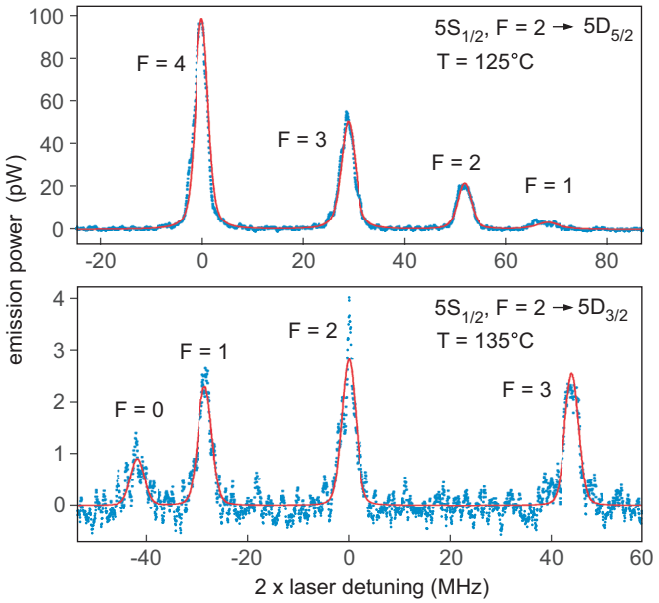

FIG. 3. Spectrum of the $5D_{5/2}$ level and the $5D_{3/2}$ level detected with the blue filter. "2x" laser detuning refers to the difference between twice the laser frequency and the Bohr frequency of the $5S$-$5D$ energy difference. The solid black line is a fit with four individual Voigt profiles. The temperature corresponds to the densities where the blue emission has a maximum. At these densities the resonance lines are already broadened in parts by collisions.

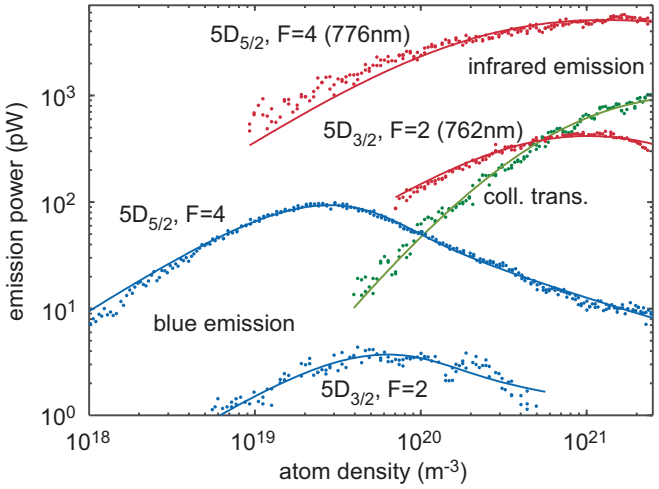

FIG. 4. Light power emitted by the atoms into the solid angle of detection at various atom densities. The laser drives transitions from $5S_{1/2}$, $F = 2$ to $5D_{5/2}$, $F = 4$ and to $5D_{3/2}$, $F = 2$. The wavelengths in brackets denote the filters used for detecting the emission. The third infrared curve labeled "coll.trans." is recorded by exciting the atoms to the $5D_{5/2}$, $F = 4$ state and detecting the infrared emission at 762 nm. It demonstrates the effect of fine-structure changing collisions. The solid lines of the infrared data are the results of the model described in Secs. IV and V. The solid lines of the blue emission are derived from a reabsorption model described in the Appendices for completeness.

762 nm. In contrast to the blue emission, the infrared emission is not limited by reabsorption and the emitted power increases with density up to a level of 5000 pW at 2×10^{21} m^{-3} which is 50 times higher than 100 pW obtained in the maximum of blue emission at a density of 2×10^{19} m^{-3}. Even at this low density, the infrared emission for $5/2$ excitation is still about seven times stronger because of the above discussed more favorable branching ratio and reabsorption of the blue emission.

At high densities the infrared emission saturates. This can be explained in parts by collisional broadening [12]. The thermal bath of neighboring ground-state atoms perturbs the optical excitation via resonant and nonresonant van der Waals interaction resulting in a broadening of the optical resonance linearly increasing with atom density. Collisional broadening leads to saturation but it does not explain the observed decrease of the emission at high densities most pronounced for $3/2$ excitation. Therefore, also collisional losses have to be taken into account. A colliding pair, one in the excited state and one in the ground state, may change its molecular potential by nonadiabatic transition at avoided crossings [13,14]. Hyperfine-structure changing, fine-structure changing, and even Coulomb changing collisions [15] are possible this way. Also a reverse pooling process [15,16] may play a role where the two atoms leave the collision both excited at the $5P$ level. To prove the importance of fine-structure changing collisions in our system we detect $5/2$ excitation with the filter for 762 nm (Fig. 4, curve labeled "coll. trans."). Since this wavelength is only emitted if the $5D_{3/2}$ level is populated, there must be collision induced population transfer from $5D_{5/2}$ to $5D_{3/2}$. In fact, it turns out that the emitted power at 762 nm is only five times smaller than the power directly emitted from $5D_{5/2}$ at 776 nm. Fine-structure changing collisions are obviously important. Because of the small energy difference between the two levels one would expect a similarly strong transfer from $5D_{3/2}$ to $5D_{5/2}$. This process is difficult to observe directly since it is hard to distinguish the collision induced emission near 776 nm from the emission caused by direct optical decay of the excited $5D_{3/2}$ level to the $5P_{3/2}$ level at the same wavelength.

IV. COLLISIONAL BROADENING

Collisional effects can be investigated more directly by looking at the linewidth of the resonances. Figure 5 shows the observed full width at half maximum versus density. Note that the linewidth refers to twice the laser frequency. For $3/2$ excitation collisional broadening is smallest and the same for all four resonances of the hyperfine multiplet. Here, we only show the $F = 2$ resonance. For $5/2$ excitation the curves deviate from a strictly linear increase. This is surprising since collisional broadening should be proportional to the collision rate, which grows linear with density:

$$W = \beta n + \gamma_{\text{eff}}. \tag{1}$$

Here W, β, n, and γ_{eff} are the full width at half maximum, the broadening coefficient, the number density, and the linewidth at low density when collisions can be neglected. However, it is well known that for nonresonant broadening the broadening coefficient may explicitly depend on the temperature T of the gas, $\beta = \beta(T)$. Detailed studies for instance exist for metastable helium in gas discharges where density and

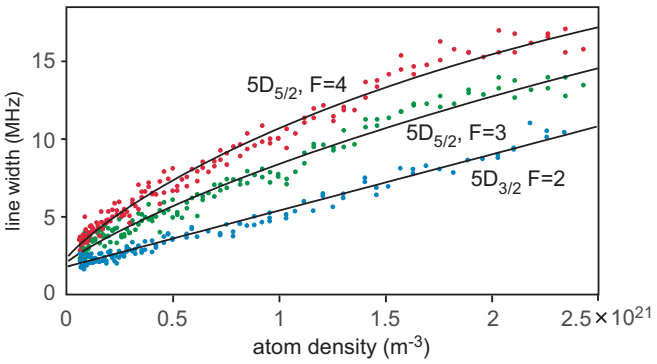

FIG. 5. Full width at half maximum of the resonances vs density for the resonances of the $5D_{5/2}$ multiplet with $F = 4$, 3 and the resonance of the $5D_{3/2}$ multiplet with $F = 2$. The solid lines are obtained by fitting Eq. (2) to the experimental data.

temperature can be varied independently [17]. In our experiment we vary the density by changing the cell temperature so that β may also change. We capture this yet unknown property of the rubidium two-photon transition with an ansatz linear in temperature, $\beta(T) = m - cT$, and fit the expression

$$W(n, T) = (m - cT)n + \gamma_{\text{eff}} \tag{2}$$

to our data. The values for the fit parameters m, c, and γ_{eff} are shown in Table I. For the two-photon transition in rubidium the temperature dependence of β has not yet been discussed in literature and we cannot compare the values of m and c to other work. It is interesting that the temperature dependence varies with the hyperfine quantum number F and that a significant effect is observed only for the resonances of the $5D_{5/2}$ level. A simple and intuitive explanation appears to be difficult and one might be forced to carry out a full calculation, a project that is beyond the scope of this paper [18]. At low densities the line shape follows a Voigt profile with a Gaussian part due to transit broadening and laser linewidth and a Lorentzian part due to the natural decay rate. From a detailed analysis of our setup we expect a linewidth of 1.8 MHz, which agrees well with the fitted values of $\gamma_{\text{eff}} \simeq 2$ MHz.

We can now use the linewidth data as described by Eq. (2) to interpret the emission curves in Fig. 4. The $5S$-$5P$-$5D$ ladder system may be treated as an effective two level system since the intermediate $5P$ level is far detuned and can be adiabatically eliminated [19]. The power $P(n)$ emitted by the atoms is proportional to the product of the density n and the population ρ of the excited $5D$ state:

$$P(n) \propto n\rho. \tag{3}$$

According to the two level Bloch model [20] the population can be written as

$$\rho(\delta) = \frac{1}{2}\frac{\Omega^2\Gamma_2}{\Gamma_1(\delta^2 + \Gamma_2^2) + \Omega^2\Gamma_2}. \tag{4}$$

Here, δ denotes the detuning of the laser from resonance and Ω is the effective Rabi frequency for the two-photon transition [19]. The population decay rate Γ_1 and coherence decay rate Γ_2 depend on density due to collisions. In our experiment the effective Rabi frequency is smaller than the decay rates, $\Omega^2 \ll \Gamma_2\Gamma_1$, and the expression reduces to

$$\rho(\delta) \simeq \frac{1}{2}\frac{\Omega^2\Gamma_2}{\Gamma_1}\frac{1}{\delta^2 + \Gamma_2^2}. \tag{5}$$

This Lorentz-type resonance function has a full width at half maximum of $W = 2\Gamma_2/2\pi$ such that Γ_2 can be obtained directly from Eq. (2):

$$\Gamma_2 = \pi W = \pi[(m - cT)n + \gamma_{\text{eff}}]. \tag{6}$$

For Γ_1 we make the ansatz

$$\Gamma_1 = \alpha n + \gamma_{5d} \tag{7}$$

with the natural decay rate of the $5d$ states $\gamma_{5d} = 4.2 \times 10^6\ \text{s}^{-1}$ [8] and the collisional loss coefficient α to be determined from our observation. On resonance ($\delta = 0$) the emitted power reads

$$P(n) \propto n\rho(0) = n\frac{1}{2}\frac{\Omega^2}{\Gamma_2\Gamma_1} \tag{8}$$

and after inserting Eqs. (6) and (7) one obtains

$$P(n) \propto \frac{1}{2\pi}\frac{\Omega^2 n}{[(m - cT)n + \gamma_{\text{eff}}](\alpha n + \gamma_{5d})}. \tag{9}$$

The detected power $P_d(n)$ is proportional to the emitted power $P(n)$ such that

$$P_d(n) = A\frac{n}{[(m - cT)n + \gamma_{\text{eff}}](\alpha n + \gamma_{5d})}. \tag{10}$$

The prefactor A and the collisional loss coefficient α can be determined by fitting this expression to the observed emission. Some of these fits are shown as red solid lines in Fig. 4. The fit parameters are presented in Table II. The prefactor A depends on the effective Rabi frequency of the specific two-photon transition and on the details of the detection setup, which we do not analyze here.

V. COLLISIONAL TRANSFER

We interpret the collisional transfer (green dots in Fig. 4) with a rate model. The emitted light power at 762 nm is

TABLE I. Fit parameters for the observed collisional broadening. The width of the excitation into the $5D_{3/2}$ level grows linearly with density and shows no observable temperature dependence. c was thus fixed to zero.

Excited level	m (10^{-21} MHz m^3)	c (10^{-23} MHz m^3/ K)	γ_{eff} (MHz)
$5D_{5/2}$, $F = 4$	55 ± 0.7	9.8 ± 0.2	2.3 ± 0.6
$5D_{5/2}$, $F = 3$	32 ± 0.8	5.4 ± 0.2	2.0 ± 0.7
$5D_{3/2}$, $F = 2$	3.6 ± 0.5		1.8 ± 0.5
$5D_{3/2}$, $F = 3$	3.5 ± 0.5		1.8 ± 0.4

TABLE II. Emission strength A and collisional loss coefficient α.

Excited level	A (10^{-10} pW m^3 s^{-2})	α (10^{-15} m^3 s^{-1})
$5D_{5/2}$, $F=4$	3.7 ± 0.4	2.7 ± 0.8
$5D_{5/2}$, $F=3$	2.2 ± 0.2	2.8 ± 0.7
$5D_{3/2}$, $F=2$	0.12 ± 0.01	1.7 ± 0.6
$5D_{3/2}$, $F=3$	0.09 ± 0.01	1.8 ± 0.7

proportional to the number $N_{3/2}$ of atoms in the $5D_{3/2}$ level. Its change

$$\dot{N}_{3/2} = -(\gamma_{5D} + \kappa_{3/2} n) N_{3/2} + \Phi \tag{11}$$

is given by optical decay and collisional losses (first term on the right side) and the collision transfer rate Φ. The loss coefficient $\kappa_{3/2}$ may slightly deviate from the above determined value of the loss coefficient α for the $5D_{3/2}$ level because different to optical excitation collisions populate several hyperfine states of the $5D_{3/2}$ level each decaying with an individual collisional loss coefficient. Here, we describe them as a single state with an effective coefficient $\kappa_{3/2}$. In equilibrium

$$N_{3/2} = \frac{\Phi}{\gamma_{5D} + \kappa_{3/2} n}. \tag{12}$$

Since the transfer involves a collision of a ground-state atom with an atom in the optically excited $5D_{5/2}$ level, Φ can be written as

$$\Phi = N_{5/2} \sigma_c n v \tag{13}$$

with $N_{5/2}$, σ_c, and v being the number of atoms in the excited $5D_{5/2}$ level, the transfer cross section, and the relative velocity of the colliding atoms, respectively. With this we obtain

$$N_{3/2} = \frac{N_{5/2} \sigma_c n v}{\gamma_{5D} + \kappa_{3/2} n}. \tag{14}$$

We are interested in the ratio R of light power emitted from the $5D_{3/2}$ level and the $5D_{5/2}$ level. Since both levels decay into the $5P$ level with the same rate, this ratio is given by the number ratio of excited atoms:

$$R = \frac{N_{3/2}}{N_{5/2}} = \sigma_c v \frac{n}{\gamma_{5D} + \kappa_{3/2} n}. \tag{15}$$

We fit this expression to the experimental data (ratio of the green data points and the upper red data points in Fig. 4) and obtain values for $\sigma_c v$ and $\kappa_{3/2}$ given in Table III. The experimental ratio and the fitted expression are shown in Fig. 6. By comparing the transfer rate coefficient $\sigma_c v$ to the total loss coefficient α of the $5D_{5/2}$ level we find that about a third of its collisional losses are due to transfer to the $5D_{3/2}$ level.

The explicit density dependence of the power emitted from $5D_{3/2}$ level can now be taken from Eq. (14) with $N_{5/2}$ being proportional to $P(n)$ given by Eq. (9). The solid green line in Fig. 4 shows the result with the prefactor determined by a simple fit.

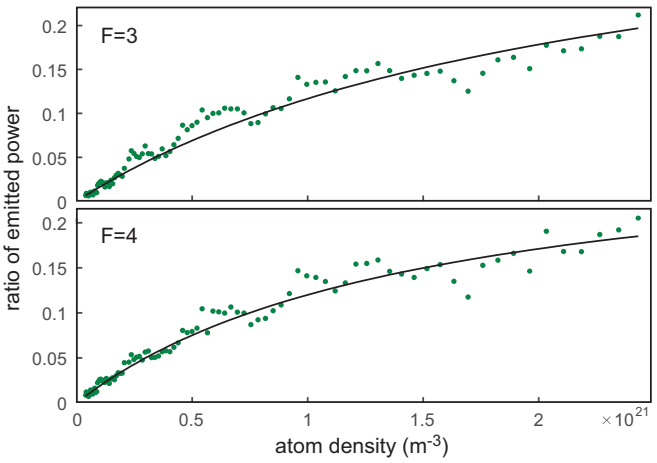

FIG. 6. Ratio of the observed emitted power at 762 and 776 nm for optical excitation into $5D_{5/2}$, $F = 3$ and 4. The solid lines are fits according to Eq. (15).

In Tables I–III the relative confidence intervals of the fit parameters noted in brackets typically stay below 50%. The largest contribution to the systematic errors comes from temperature calibration since the density strongly depends on the rubidium vapor pressure. A miscalibration of about 10 K shifts the fit parameters outside their confidence intervals. However, we are convinced that such a large miscalibration is not realistic in our setup. The uncertainty with which the vapor pressure can be derived from temperature is reported to be 5% [11]. This adds to the systematic error on a similar level.

VI. CONCLUSION AND OUTLOOK

In summary, we have observed strong infrared emission at 762 and 776 nm during Doppler-free two-photon laser excitation of the $5D$ levels in ^{87}Rb. We have recorded data in a thermal vapor cell up to a maximum vapor pressure of 130 mTorr. The emitted infrared power exceeds the blue emission by up to a factor of 50 and is limited at high densities by collisional broadening of the resonances and by losses due to collisional energy transfer. The observations reveal a yet unknown temperature dependence of the broadening coefficients for the hyperfine states of the $5D_{5/2}$ level. We also directly observed strong collisional energy transfer from the upper to the lower $5D$ fine-structure level. Since the resulting emission at 762 nm can easily be separated from the laser stray light, it becomes an attractive alternative for detecting the two-photon transition at high densities.

TABLE III. Collisional transfer rate coefficient $v\sigma_c$, corresponding cross section σ_c for $v = 300$ m s^{-1}, and collisional loss coefficient $\kappa_{3/2}$.

Optically excited level	$v\,\sigma_c$ (10^{-16} m^3 s^{-1})	σ_c (10^{-14} cm^2)	$\kappa_{3/2}$ (10^{-15} m^3 s^{-1})
$5D_{5/2}$, $F=4$	8.4 ± 0.3	2.8 ± 0.7	2.8 ± 0.8
$5D_{5/2}$, $F=3$	7.1 ± 0.2	2.4 ± 0.6	1.9 ± 0.8

It is interesting that the cross section for reverse pooling of $2 \times 10^{-14}\,\mathrm{cm}^2$ [15] is close to our value for collisional transfer. Obviously, this effect also significantly contributes to the collisional losses of the $5D$ level. Reverse pooling results in two excited atoms in the $5P$ level, which optically decay into the ground state such that each excitation to the $5D$ level generates two infrared photons. Furthermore, also the lower part of the optical decay cascade via the $5P$ level generates extra infrared photons. Consequently, there should be strong emission also at 780 and 795 nm. In fact, if filters are removed we observe an increased atomic emission signal which cannot be explained by the filters' insertion losses alone. Without filter the signal contains all blue and infrared emission. Furthermore, signal reduction by reabsorption of the blue light is partly suppressed since the reabsorbed photon may reappear as an infrared photon after decay from the $6P$ level to the $5P$ level via $6S$ and $4D$. It thus seems that the best detection efficiency may be achieved with a narrowband interference filter that only cuts out laser stray light. At high densities a 300 times improved detection efficiency appears feasible.

Concerning a possible optimization of the rubidium secondary frequency standard, operation at high densities has the disadvantage of collisional linewidth broadening by about a factor of 10. At high densities also collision induced light shift [5] has to be taken into account. Depending on the specific requirements of the frequency standard (accuracy, speed, size, portability, power consumption, cost, etc.) the optimum density varies. For the stabilization of a laser small integration time of a strong signal might be more important than long-term temperature dependent drift due to collisional shift. For best accuracy, small linewidth and thus low density is desirable. However, also the light shift should be small. This requires small laser power and thus high detection efficiency at high density. In this case a moderate density might be best and one can at least take advantage of the seven times higher infrared emission in the commonly used density regime where blue emission has its maximum (see Sec. III). Finally, we would like to mention that at high density the two-photon transition can also be observed by absorption. On resonance we observe a 0.1% reduction of the light power transmitted through the cell (see "absorption detection" in Fig. 2). In combination with a lock-in recording technique a simplified and very compact design should be possible.

ACKNOWLEDGMENT

This work has been supported by Deutsche Forschungsgemeinschaft Grant No. ZI 419/9-1.

APPENDIX A: REABSORPTION

The atoms excited by the laser emit a Doppler broadened spectrum near 420 nm which is partially absorbed by the dense gas between the laser defined excitation volume and the wall of the vapor cell. We assume that the absorbing atoms scatter the absorbed energy either in a direction or at a wavelength not seen by the detector. Forward scattering into the direction of the detector is small and can be neglected. According to the two level Bloch model for the $5S$-$6P$ transition the scattered power per atom P_s is given by the equilibrium population of the excited state multiplied by the excitation energy $\hbar\omega$ and the excited-state decay rate γ . We neglect collisions and power broadening and obtain

$$P_s = \frac{I}{I_s}\hbar\omega\gamma/2\frac{(\gamma/2)^2}{(\delta - kv)^2 + (\gamma/2)^2}, \tag{A1}$$

with the frequency ω of the absorbed light, the Bohr frequency ω_0, the detuning $\delta = \omega - \omega_0$, and the saturation intensity I_s. The Doppler shift kv contains the wave number k and the velocity component v of the scatterer along the direction towards the detector. The absorbing volume can be written as the product of a cross section A and a thickness d. We decompose this volume in small slices of thickness Δz and ask about the intensity change ΔI after passing one such slice. For a given density n there are $nA\Delta z$ atoms in the slice which scatter a power of $P = \Delta IA = P_s nA\Delta z$. The limit for small Δz yields a differential equation for the intensity along the path from the excitation volume to the cell wall,

$$\frac{\Delta I}{\Delta z} \to \frac{dI}{dz} = -nP_s, \tag{A2}$$

and after summing over the velocity distribution one gets

$$\frac{dI}{dz} = -\frac{n}{\sqrt{\pi}v_0}\frac{\hbar\omega\gamma}{2}\frac{I}{I_s}\int_{-\infty}^{\infty} e^{-v^2/v_0^2}\frac{(\gamma/2)^2}{(\delta - kv)^2 + (\gamma/2)^2}dv \tag{A3}$$

with average thermal velocity $v_0 = \sqrt{2k_BT/m}$. The integrand contains a broad Gaussian and a narrow Lorentzian part. As a good approximation one can shift the Gaussian part outside the integral and evaluate it at the maximum of the Lorentz function, $v = \delta/k$. The remaining integral can be solved, leading to

$$\frac{dI}{dz} = -\frac{\sqrt{\pi}}{4}\frac{\hbar\omega\gamma^2}{I_s v_0 k}n\exp\left[-\left(\frac{\delta}{kv_0}\right)^2\right]I(z). \tag{A4}$$

The solution of this equation is

$$I(n, \delta, d) = I_0\exp(-ane^{-(\delta/\delta_{\mathrm{th}})^2}) \tag{A5}$$

with the abbreviations

$$a := \frac{\sqrt{\pi}}{4}\frac{\hbar\omega\gamma^2}{I_s\delta_{\mathrm{th}}}d$$

and

$$\delta_{th} := v_0 k.$$

It describes the spectral filtering by the scatterers along the distance d between the excitation volume and the cell wall.

We write the spectrum emitted by the atoms in the excitation volume as a Doppler-broadened Gaussian:

$$S(\delta) = S_0\exp[-(\varepsilon\delta/\delta_{\mathrm{th}})^2], \tag{A6}$$

with some prefactor S_0 and a parameter ε close to 1, which takes small additional broadening into account such as instrumental resolution, natural linewidth, and collisional broadening. At the detector the spectrum $S_d(\delta)$ of the filtered light is proportional to the product of the emission and the absorption spectrum:

$$S_d(\delta) \propto e^{-(\varepsilon\delta/\delta_{\mathrm{th}})^2}\exp(-ane^{-(\delta/\delta_{\mathrm{th}})^2}). \tag{A7}$$

The scattering atoms filter out the central part of the emission spectrum and allow only some light from the slopes of the emission spectrum to pass to the detector. The total transmitted power at the detector is obtained by summing over all frequencies:

$$P_d \propto \int_{-\infty}^{\infty} e^{-(\varepsilon\delta/\delta_{\rm th})^2} \exp(-ane^{-(\delta/\delta_{\rm th})^2}) d\delta. \qquad \text{(A8)}$$

This expression was fitted to the observation with a, ε, and a prefactor as fit parameters (blues solid lines in Fig. 4). For the $5/2$ excitation into $F = 4$ one obtains $a = 5.5 \times 10^{-20}$ m^3 and $\varepsilon = 1.3$. The fitted value for a perfectly fits to the theoretically expected value of $a = 5.4 \times 10^{-20}$ m^3. For the $3/2$ excitation into $F = 2$ the fit quality is not as good and $\varepsilon = 1.1$.

APPENDIX B: COMPARISON TO OTHER WORK

We compare our observations to other related work. In rubidium, collisional broadening has been experimentally investigated for two-photon transitions into Rydberg states with principle quantum number between $q = 10$ and 60 [21]. This paper observes an almost linear behavior of the broadening coefficient with q for $q < 20$. Extrapolating these data down to $q = 5$ yields 4×10^{-21} MHz m^3 in good agreement with our observed broadening of the $3/2$ excitation (Table I).

For ^{85}Rb in a natural isotope mixture broadening of the $5/2$ excitation has been observed with a broadening coefficient of 79 kHz/mTorr with respect to the laser frequency [22]. With respect to the excitation energy (factor of 2) and after transforming pressure into density this corresponds to a broadening coefficient of 6.9×10^{-21} MHz m^3. To compare this value to our observed temperature-dependent coefficient we force a linear fit to our data and obtain a slope of 10×10^{-21} and 7.6×10^{-21} MHz m^3 for the resonances with $F = 4$ and 3, respectively. Again the agreement is well within the error margin. Energy transfer and collision-induced losses have been treated for rubidium in detailed calculations [13], however, without taking the hyperfine structure into account. With a thermally averaged relative velocity of about $\bar{v} = 300$ m s^{-1} our typical observed loss coefficient of $\alpha \approx 2 \times 10^{-15}$ m^3 s^{-1} translates into a cross section of $\sigma \approx 4 \times 10^{-14}$ cm^2. This is compatible with the theoretical values. In particular our observed cross section $\sigma_c = 2.8 \times 10^{-14}$ cm^2 agrees well with the theoretical cross section of 3.1×10^{-14} cm^2 for collisional transfer between $5D_{5/2}$ and $5D_{3/2}$.

[1] F. Nez and F. Biraben, Opt. Commun. **102**, 432 (1993).
[2] Y. Millerioux, D. Touahri, L. Hilico, A. Clairon, R. Felder, F. Biraben, and B. de Beauvoir, Opt. Commun. **108**, 91 (1994).
[3] D. Touahri, O. Acef, A. Clairon, J.-J. Zondy, R. Felder, L. Hilico, B. de Beauvoir, F. Biraben, and F. Nez, Opt. Commun. **133**, 471 (1997).
[4] O. Terra and H. Hussein, Appl. Phys. B **122**, 27 (2016).
[5] K. W. Martin, G. Phelps, N. D. Lemke, M. S. Bigelow, B. Stuhl, M. Wojcik, M. Holt, I. Coddington, M. W. Bishop, and J. H. Burke, Phys. Rev. Appl. **9**, 014019 (2018).
[6] M. T. Hummon *et al.*, Optica **5**, 443 (2018).
[7] C. Perrella, P. S. Light, J. D. Anstie, T. M. Stace, F. Benabid, and A. N. Luiten, Phys. Rev. A **87**, 013818 (2013).
[8] D. Sheng, A. Pérez Galván, and L. A. Orozco, Phys. Rev. A **78**, 062506 (2008).
[9] K. W. Martin, B. Stuhl, J. Eugenio, M. S. Safronova, G. Phelps, J. H. Burke, and N. D. Lemke, Phys. Rev. A **100**, 023417 (2019).
[10] A. Lindgård and S. E. Nielsen, At. Data Nucl. Data Tables **19**, 533 (1977).
[11] S. A. Steck, Rubidium 87 D line data, http://steck.us/alkalidata (revision 2.2.2, 9 July 2021), original data in C. B. Alcock *et al.*, Canadian Mettallurgical Quarterly **23**, 3009 (1984).
[12] M. Baranger, Phys. Rev. **111**, 481 (1958).
[13] K. Orlovsky, V. Grushevsky, and A. Ekers, Eur. Phys. J. D **12**133 (2000).
[14] K. Burnett, Phys. Rep. **118**, 339 (1985).
[15] L. Caiyan, A. Ekers, J. Klavins, and M. Jansons, Phys. Scr. **53**, 306 (1996).
[16] L. Barbier and M. Chéret, J. Phys. B **16**, 3213 (1983).
[17] A. Atiola, B. C. Gibson-Wilde, A. C. Lindsay, J. L. Nicol, and I. B. Whittingham, J. Phys. B **21**, 249 (1988).
[18] As alternative explanation for the observed hyperfine and temperature dependence of the linewidths one may speculate about additional noncollisional broadening effects that are significant only for the strongest transitions with highest photon scattering rate. Here we just like to note that we have observed the same linewidth versus density curves for blue light detection, infrared light detection, and even in absorption. The linewidth curves also do not depend on laser power.
[19] A. Sinatra, F. Castelli, L. A. Lugiato, P. Grangier, and J. Ph. Poizat, Opt. **7**, 405 (1995).
[20] W. Vogel, and D.-G. Welsch, *Quantum Optics* (Wiley, New York, 2006), p. 372.
[21] K.-H. Weber and K. Niemax, Opt. Commun. **31**, 52 (1979); similar data have been published later by B. P. Stoicheff and E. Weinberger, Phys. Rev. Lett. **44**, 733 (1980).
[22] N. D. Zameroski, G. D. Hager, C. J. Erickson, and J. H. Burke, J. Phys. B **47**, 225205 (2014).